Identification of the N- and C-Terminal Substrate Binding Segments of Ferredoxin-NADP$^+$ Reductase by NMR[†,@]

Masahiro Maeda,[‡,§,||] Young Ho Lee,[‡] Takahisa Ikegami,[‡] Kohsuke Tamura,[‡] Masaru Hoshino,[‡] Toshio Yamazaki,[⊥] Masato Nakayama,[‡] Toshiharu Hase,[‡] and Yuji Goto*[,‡,§]

Institute for Protein Research, Osaka University, Yamadaoka 3-2, Suita, Osaka 565-0871, Japan, CREST, Japan Science and Technology Agency, Saitama, Japan, and Genomic Sciences Center, RIKEN Yokohama Institute, 1-7-22 Suehiro-cho, Tsurumi-ku, Yokohama 230-0045, Japan

Received March 6, 2005; Revised Manuscript Received June 13, 2005

ABSTRACT: Ferredoxin-NADP$^+$ reductase (FNR) catalyzes the reduction of NADP$^+$ through the formation of an electron transfer complex with ferredoxin. To gain insight into the interaction of this enzyme with substrates at both ends of the polypeptide chain, we performed NMR analyses of a 314-residue maize leaf FNR with a nearly complete assignment of the backbone resonances. The chemical shift perturbation upon formation of the complex indicated that a flexible N-terminal region of FNR contributed to the interaction with maize ferredoxin, and an analysis of N-terminally truncated mutants of FNR confirmed the importance of this region for the binding of ferredoxin. Comparison between the spectra of FNR in the NADP$^+$- and inhibitor-bound states also revealed that the nicotinamide moiety of NADP$^+$ was accessible to the C-terminal Tyr314. We propose that the formation of the catalytic competent complex of FNR and substrates is achieved through the interaction of the N- and C-terminal segments with ferredoxin and NADP$^+$, respectively. Since the ends of the polypeptide chain act as flexible regions of proteins, they may contribute to the search of a larger space for a binding partner and to the opening of active sites.

Ferredoxin-NADP$^+$ reductase (FNR)[1] is a flavin adenine dinucleotide (FAD)-containing protein that catalyzes the transfer of electrons from ferredoxin (Fd) to NADP$^+$ (*1*, *2*). In higher plants, the production of NADPH catalyzed by FNR is the last step of the photosynthetic I chain (*3*, *4*). FNRs have also been isolated from a variety of tissues and organisms with both phototrophic and heterotrophic metabolisms (*5*). The interaction and electron transfer between FNR and its various substrates are reported. In nonphotosynthetic bacteria and eukaryotes, the reaction is driven toward Fd or flavodoxin reduction, providing electrons for metabolisms as diverse as steroid hydroxylation in mammalian mitochondria (*6*), methane oxidation in methanotrophic bacteria (*7*), and reductive activation of biosynthetic enzymes in *Escherichia coli* and other prokaryotes (*8*). In addition, FNR has two isoenzymes in leaves and roots, suggesting an efficient electron flux of the NADPH−FNR−Fd cascade and metabolism in nonphotosynthetic organs (*9*, *10*).

High-resolution structures of several FNRs and enzyme−substrate complexes have been determined by X-ray crystallography (*11*−*14*). The structures of FNRs appear to be the prototype of a two-domain structural motif that occurs in many enzymes transferring electrons via a nicotinamide dinucleotide. This large family of flavoprotein reductases and oxidases is defined by six segments of highly conserved residues (*5*, *11*). The contact mode of Fd and FNR indicated that both electrostatic and hydrophobic packing forces are important for formation of the productive complex (*15*, *16*). Mutagenesis studies revealed that the charged residues in the three conserved surfaces of *Anabaena* FNR play a role for electron transfer between FNR and Fd (*17*). On the other hand, another substrate, NADP$^+$, interacts with the C-terminal region of FNR. The 2′-phospho-AMP and pyrophosphate portions of the NADP$^+$ are bound to the edge of the β-sheets in the NADP$^+$ binding domain (*12*, *14*, *18*). However, the orientation of the nicotinamide moiety was reported with three kinds of conformations, probably due to the steric constraint in the C-terminal region of FNR (*18*). The crucial C-terminal tyrosine (Tyr314) side chain is well stabilized by a stacking interaction with the isoalloxazine ring of FAD in wild-type FNR, whereas the functional hydride transfer from FAD to NADP$^+$ could only be achieved by disruption of the stacking interaction of the tyrosine side chain with the isoalloxazine ring (*4*). The crystals of the complexes of FNR in the productive binding mode with NADP$^+$ were only observed with an engineered pea FNR protein in which the C-terminal tyrosine was replaced with a nonaromatic serine residue (*14*). However, the absence of a phenol ring at the C-terminal position resulted in a significant decrease in the extent of catalysis (*19*).

[†] This work was supported by Grants-in-aid for Scientific Research from the Japanese Ministry of Education, Culture, Sports, Science and Technology.

[@] The resonance assignments for the free FNR have been deposited in the BioMagResBank under BMRB accession number 6695.

* To whom correspondence should be addressed: Institute for Protein Research, Osaka University, Yamadaoka 3-2, Suita, Osaka 565-0871, Japan. Telephone: +81-6-6879-8614. Fax: +81-6-6879-8616. E-mail: ygoto@protein.osaka-u.ac.jp.

[‡] Osaka University.

[§] CREST, Japan Science and Technology Agency.

[||] Present address: Laboratory of Biochemistry, Department of Chemistry, Graduate School of Science, Nagoya University, Chikusa-ku, Nagoya 464-8602, Japan.

[⊥] RIKEN Yokohama Institute.

[1] Abbreviations: FNR, ferredoxin-NADP$^+$ reductase; Fd, ferredoxin; FAD, flavin adenine dinucleotide; TROSY, transverse relaxation optimized spectroscopy; HSQC, heteronuclear single-quantum coherence.

10.1021/bi050424b CCC: $30.25
Published on Web 07/09/2005

Despite the fact that the enzymatic properties of FNR have been extensively characterized in both X-ray crystallography and biochemical studies, most consideration of its catalytic mechanism has been focused on the rigid core region of the molecule. FNR has a highly flexible disordered tail at the N-terminus in the FAD-binding domain, which was not visible in the electron density map (*11*, *16*). Although NMR analysis can detect weak interactions, including mobile regions, no multidimensional NMR study of FNR has been reported to date. This is because the large number of residues and the molecular mass of FNR (314 residues, 35 kDa) hamper straightforward NMR analyses. The development of advanced NMR techniques (*20*, *21*) has made it possible to assign the backbone resonances of enzymes (*22*−*24*) composed of more than 300 residues. In this study, we report the NMR analyses of a 314-residue maize leaf FNR with nearly complete assignments (≈95%) of the backbone resonances. Information about FNR polypeptide termini obtained from chemical shift perturbation analyses and mutagenesis has clarified an additional location of the ferredoxin binding site and the NADP$^+$ binding mechanism in solution.

MATERIALS AND METHODS

Sample Preparation for NMR Measurements. The wild-type FNR proteins for the NMR analyses were obtained by overexpression in cultures of *E. coli* TG1 cells transformed with the pYOL-FNR1 plasmid (*9*). In the preparation of a uniformly ^{2}H-, ^{13}C-, and ^{15}N-labeled FNR, a colony from the transformed cells was grown in 50 mL of Luria-Bertani medium with 0.14 mM ampicillin at 37 °C for 8 h, and then 10 mL of *E. coli* was inoculated with 1.5 L of M9 medium containing 80% ^2H_2O supplemented with 1.24 g/L $(^{15}NH_4)_2SO_4$ and 2 g/L [^{13}C]glucose. The isotopic reagents were purchased from Shoko Co., Ltd., and ^2H_2O (99.9%) was from Isotec. When the cell density reached the absorbance of 0.65 at 600 nm, 1 mM IPTG was added for induction, and the bacteria were grown for an additional 12 h. The ^{2}H-, ^{13}C-, and ^{15}N-labeled FNR was purified as described previously (*9*). The final yield of ^{2}H-, ^{13}C-, and ^{15}N-labeled protein was 18.5 mg. To protonate the deuterated amide groups, purified 4 μM ^{2}H-, ^{13}C-, and ^{15}N-labeled FNR was incubated in a 25 mM sodium phosphate buffer containing 2 M urea at pH 8.0 and 40 °C for 48 h. This treatment was required for obtaining high-quality spectra for the main-chain resonance assignment (*23*, *24*), since the procedure promoted the D−H exchange of the highly protected amide deuterons with the solvent protons, making it possible to observe 31 additional amide resonances. To remove the urea after the protonation treatment, the concentrated protein was passed through a PD-10 gel filtration column (Amersham Biosciences) pre-equilibrated with the buffer solution for subsequent NMR measurements.

NMR Spectroscopy and Backbone Resonance Assignments. NMR experiments for the resonance assignments of the backbone atoms were performed at 40 °C with an 800 MHz spectrometer (Bruker DRX800) equipped with a 5 mm triple-resonance probe head with triple-axis gradient coils. A cryogenic probe head with a one-axis z-gradient coil was also used for measurements. The NMR samples for the backbone resonance assignments comprised 1 mM isotopically labeled FNR dissolved in a 25 mM sodium phosphate buffer (pH 8.0) containing 5% ^2H_2O for the NMR lock and 0.05% NaN_3. For the measurement at pH 6.5, 50 mM sodium perchlorate ($NaClO_4$) was added to a 0.4 mM protein sample. The 50 mM $NaClO_4$ was useful in preventing the aggregation of FNR at pH 6.5, probably because of its chaotropic effects. The sample (volume of 250 μL) was injected into a 5 mm ϕ Shigemi microtube. The ^{1}H, ^{15}N, and ^{13}C resonances of the backbone atoms except for the N-terminal region were assigned by a combination of multidimensional and multinuclear TROSY-based and deuterium-decoupled experiments at both pH 8.0 and 6.5: TROSY-HSQC, TROSY-HNCACB, TROSY-HN(CO)CACB, TROSY-HN(CA)CO, and TROSY-HNCO (*25*, *26*). For the backbone assignment of the highly flexible N-terminal region (Ile1−Lys17), the CBCANH (*27*) spectrum was measured using nondeuterated 1 mM ^{13}C- and ^{15}N-labeled FNR dissolved in a 25 mM sodium phosphate buffer (pH 6.0) containing 50 mM $NaClO_4$, 5% ^2H_2O, and 0.05% NaN_3. To confirm the sequential backbone assignment, [α-^{15}N]Lys- or [α-^{15}N]Arg-labeled FNR was used to measure ^{1}H−^{15}N HSQC spectra where only the peaks from these selective amino acids appeared. The base frequency was referenced with 2,2-dimethyl-2-silapentane-5-sufonic acid (DSS). All NMR spectra were processed using NMRpipe (*28*) and analyzed with PIPP (*29*). The secondary structure was estimated by the ^{13}C chemical shift deviations from the residue-specific random coil shifts (*30*).

Chemical Shift Perturbation Analysis. The ^{1}H−^{15}N HSQC spectra for the chemical shift perturbation analysis were recorded at 40 °C using 600 and 800 MHz spectrometers. The sample contained 0.19 mM [^{15}N]FNR and 0.20 mM Fd dissolved in a 25 mM sodium phosphate buffer (pH 6.0) with 50 mM $NaClO_4$. The recombinant maize leaf Fd I was prepared as described previously (*31*). For the NADP$^+$ titration experiment, the perturbation levels upon NADP$^+$ binding were low at pH 6.0, and therefore, we conducted the experiments at pH 8.0. Aliquots of 1−8 μL of 12.5−125 mM NADP$^+$ solutions were added repeatedly to 0.9 mM [^{15}N]-FNR in a 5 mm ϕ Shigemi microtube, dissolved initially in 250 μL of a 25 mM sodium phosphate buffer (pH 8.0) containing 5% ^2H_2O, until NADP$^+$ concentrations of 0.05, 0.10, 0.20, 0.39, 0.58, 0.77, 0.95, and 12.4 mM were reached. The data were analyzed using the IGOR-Pro data analysis program (WaveMetrics). An inhibitor, adenosine 2′,5′-diphosphate, was mixed with 0.19 mM [^{15}N]FNR in the same buffer at a ligand concentration of 0.2 mM. NADP$^+$ was purchased from Oriental Yeast, and adenosine 2′,5′-diphosphospate was from Sigma. The backbone ^{1}H and ^{15}N chemical shifts for the Fd- or ligand-bound FNR were assigned by tracing the corresponding peaks in ^{1}H−^{15}N HSQC spectra measured at various concentrations of Fd or ligands. To obtain the cross-peaks for the Fd-binding state of [^{15}N]FNR, Fd was mixed with 0.9 mM [^{15}N]FNR at Fd concentrations of 0.2, 0.4, 0.6, and 1 mM. Different chemical shifts observed at pH 6.0 and 8.0 were correlated by tracing the peaks in ^{1}H−^{15}N HSQC spectra measured at pH 6.0, 6.5, 7.0, 7.5, and 8.0. The protein structures were generated using MOLSCRIPT (*32*) and rendered using Raster3D (*33*). A structural model of the N-terminal fragment of FNR (Ile1−Lys18), built through the energy minimization process in Insight II/Discover (MSI), was connected to Ser19 of the atom coordinates of the FNR crystal. The conformation of the model did not necessarily reflect the actual conformation in solution.

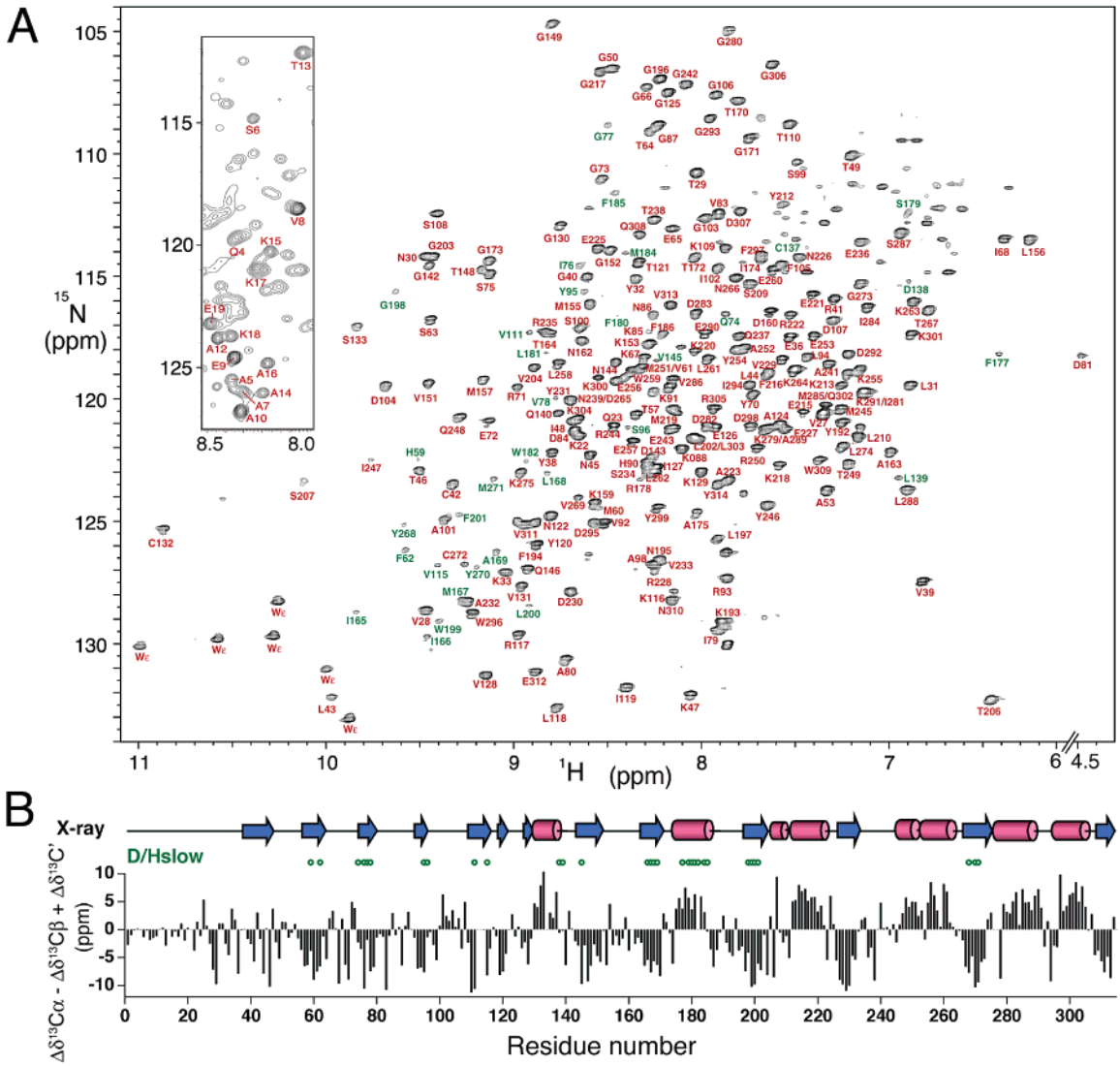

FIGURE 1: Chemical shift assignments of maize leaf FNR. (A) A ^{1}H−^{15}N TROSY-HSQC spectrum of uniformly ^{2}H-, ^{13}C-, and ^{15}N-labeled FNR measured at pH 8.0 and 40 °C. The assignments of the backbone amide signals are indicated by the single-letter codes and residue numbers. The assignments of the tryptophan side chain indoles are labeled wϵ. Green characters denote resonances with weak intensities because of incomplete amide D−H exchange without the protonation treatment of the deuterated protein. The inset is a part of the ^{1}H−^{15}N HSQC spectrum of uniformly ^{13}C- and ^{15}N-labeled FNR measured at pH 6.0 and 40 °C, displaying the resonances of the N-terminal region of FNR. The NMR spectra were prepared using NMRDraw. (B) A chemical shift deviation parameter ($\Delta\delta^{13}C_\alpha - \Delta\delta^{13}C_\beta + \Delta\delta^{13}C'$) for the $^{13}C_\alpha$, $^{13}C_\beta$, and $^{13}C'$ nuclei, where $\Delta\delta X$ represents the deviation of the observed chemical shift of nucleus X from the corresponding chemical shift when X exists in random coils. The secondary structural elements shown schematically in the top part are determined on the basis of the X-ray structure (PDB entry 1GAW). The α-helices and β-strands are colored red and blue, respectively, and the slowly exchanging amide protons mentioned in panel A are represented by green circles.

Preparation of N-Terminally Truncated FNRs. For the preparation of truncated FNR, the pYOL-FNR1 plasmid was used as a template to generate a PCR product corresponding to the FNR gene. Two truncated forms of maize leaf FNR lacking the 23 N-terminal residues (Δ23-FNR) and the 13 N-terminal residues (Δ13-FNR) were made by mutagenesis. As the sense primer, 5′-CATGCCATGGAGCCGGCCAA-GAAGGAGTCC-3′ was used for Δ13-FNR and 5′-CAT-GCCATGGATGCCGGCGTCGTCACCAAC-3′ for Δ23-FNR. These were designed to be complementary to the 5′ end of the truncation sites and to incorporate the *Nco*I site (former underline) and the *Nae*I site (latter underline). For the antisense primers of both Δ13-FNR and Δ23-FNR, 5′-CGCGGATCCCTACATTATATACGTAGTACAC-3′ was designed to be complementary to the 3′ end of the FNR gene and to incorporate the *Bam*HI site (underlined) which is located downstream of the stop codon for both Δ13-FNR and Δ23-FNR genes. The PCR product was first cloned into the pQE60 vector between the *Nco*I and *Bam*HI sites. The truncated FNRs were overexpressed with a TG1 *E. coli* strain transformed with the prepared vectors. The initial purification process of Δ13-FNR and Δ23-FNR was the same as that of wild-type FNR. The truncated FNRs were analyzed by SDS−PAGE after a bacteriolytic treatment using BugBuster (Novagen). The Fd affinity resin was prepared as described previously (*9*). In the final step of the affinity chromatography, elution of FNR was monitored by absorbance at 280 nm using the ÄKTA prime system (Pharmacia Biotech).

RESULTS

Backbone Resonance Assignments of Maize Leaf FNR. Figure 1A shows a TROSY ^{1}H−^{15}N HSQC spectrum of FNR. Almost all the backbone resonances were assigned: ^{1}H^{15}N (285 residues, 95% of total residues excluding the

N-terminus and 13 prolines), $^{13}C_\alpha$ (308 residues, 98%), $^{13}C_\beta$ (278 residues, 97%, excluding 28 glycines), and $^{13}C'$ (292 residues, 93%). The TROSY technique combined with triply labeled samples (^{2}H, ^{13}C, and ^{15}N) was introduced into the measurements for the backbone assignment, to obtain separate peaks by suppression of the amide line broadening. On the other hand, we also took advantage of the rapid ^{1}H, ^{15}N, and ^{13}C transverse relaxation effect of nondeuterated proteins using non-TROSY type pulse sequences to extract only the resonance signals with slow transverse relaxation rates arising from the highly flexible regions (Figure 1A, inset). Most of the resonance signals observed in the normal CBCANH spectrum of a protonated FNR were assigned to the 17 N-terminal residues. It should be noted that the amide resonance peaks from the N-terminal region were too broadened at pH 8.0 and 40 °C to be observed, probably because the labile amide protons exposed to the solvent, because of a high flexibility of conformation, exchanged rapidly with the solvent protons. The ^{1}H, ^{15}N, and ^{13}C chemical shifts are presented as Supporting Information.

Since the triply labeled FNR to be used for the main chain assignment was expressed in the minimum medium containing 80% D_2O, deuterons were attached to the amide nitrogens of the protein during culturing. Most of the deuterons were spontaneously exchanged with the solvent protons during the subsequent purification steps, but some of them, which were particularly highly protected from the solvent or hydrogen-bonded, remained. To effectively proceed with the exchange between amide deuterons and solvent protons, we incubated the protein in a 2 M urea solution at pH 8 and 40 °C. A circular dichroism (CD) measurement confirmed that maize leaf FNR almost retained its secondary structure, being not completely unfolded but slightly loosened enough to allow for the D−H exchange, for at least 3 days (data not shown). After the urea had been removed by gel filtration, the triply labeled FNR exhibited the same pattern of NMR resonances as ^{15}N-labeled FNR that had not been treated with urea, indicating that the conformation fully recovered after treatment with urea and then removal of it. We used nontreated samples for the other experiments, including chemical shift perturbation for the substrate bindings, for which ^{15}N-labeled, but not deuterated, samples were used.

For identifying secondary structural elements within the protein, it is useful to analyze the deviations of the obtained chemical shifts from those in random coils ($\Delta\delta$) (*30*). A parameter constructed from the chemical shift deviations ($\Delta\delta^{13}C_\alpha - \Delta\delta^{13}C_\beta + \Delta\delta^{13}C'$) of FNR was plotted against the residue number (Figure 1B), indicating that the locations of α-helices and *β*-sheets are consistent with the positions of the secondary structural elements observed in the crystal structure and that approximately 20 residues at the N-terminal end form a disordered conformation. In addition, the slowly D−H-exchanging amide protons, which are involved in hydrogen bonds, were observed in the secondary structural elements. As shown above, the parameters obtained from the NMR analyses of the solution state of FNR were almost consistent with the crystal structure. Unfortunately, two segments, each composed of three consecutive residues, were not able to be assigned because the corresponding amide signals in the spectra for the sequential connectivity were missing. Incomplete amide D−H exchanges for one of the segments in the depth of the molecule, composed of Ser112, Leu113, and Cys114, resulted in the weak intensities of the ^{1}H resonances. The other segment, composed of Gly276, Met277, and Glu278, is located at the end of helix α5 in the NADP$^+$-binding domain.

Perturbed Residues of FNR upon Formation of a Complex with Fd. FNR transfers an electron via the formation of a complex with Fd in the photosynthetic I chain. The X-ray crystal structure of the FNR−Fd complex was reported recently (*15*, *16*). Although crystallography provides useful clues about the electron transfer complex at an atomic resolution, the precise nature of the molecular interactions between FNR and Fd would be shown only in solution. Chemical shift mapping can be adapted for studying protein−protein interactions, even in a large flavoprotein complex (*34*). This technique is used to identify putative sites for interactions on a protein surface, by detecting chemical shift perturbations in ^{1}H−^{15}N HSQC NMR spectra of a uniformly labeled protein. To identify the site of interaction of Fd on FNR, chemical shift perturbations of ^{1}H−^{15}N HSQC NMR spectra of a uniformly ^{15}N-labeled FNR were detected. Figure 2A shows an overlay of the ^{1}H−^{15}N HSQC spectra recorded on 0.19 mM [^{15}N]FNR in the absence and presence of 0.2 mM Fd at pH 6.0 at 40 °C. Comparison of the spectra indicated 41 cross-peaks exhibiting significant changes upon the addition of Fd. These changes, which increased with the addition of more Fd, were classified as being in a fast exchange mode. No major line broadening depending on the Fd concentrations was observed in the ^{1}H−^{15}N HSQC spectra.

On the basis of the known resonance assignments of FNR, the chemical shift perturbations were mapped onto the tertiary structure. Largely perturbed residues were involved in the interaction with Fd. Glu312, the significant residue of FNR for interaction with Fd (*35*), was perturbed with large chemical shift changes in the presence of Fd (the residue numbering of maize and spinach leaf FNRs is identical). Mapping of the perturbation along the FNR sequence reveals that most of the perturbed residues belong to the FAD-binding domain (Ile1−Lys153), but both N- and C-terminal polypeptide segments were also greatly perturbed (Figure 2B). Figure 2C shows the mapping of the 41 markedly perturbed residues on the X-ray structure of the FNR−Fd complex. The regions with significant chemical shift changes were in good agreement with the contact surface with Fd in the crystal structure of the maize leaf FNR−Fd complex, which demonstrated intermolecular salt bridges formed by the side chains of residues Lys33, Lys88, Lys91, Glu154, and Lys304 of FNR, and hydrophobic contacts by those of Val92, Leu94, Val151, and Val313 of FNR (*16*). Thus, most of the strongly perturbed residues are on the contact surface between FNR and Fd, which is located near the electron-transferring center, composed of the isoalloxazine ring of FAD and the [2Fe-2S] cluster of Fd (Figure 2C). Since the chemical shift perturbation method does not always reflect the direct binding effect (*36*), we investigated the contribution of the disordered N-terminal region to Fd binding by the subsequent approach.

N-Terminal Truncation Study of FNR. Interestingly, the amide resonances of several N-terminal residues (Ile1−Lys17) were perturbed upon binding of Fd, as well as the well-known Fd-binding site of FNR. We investigated the contribution of the disordered N-terminal region to the

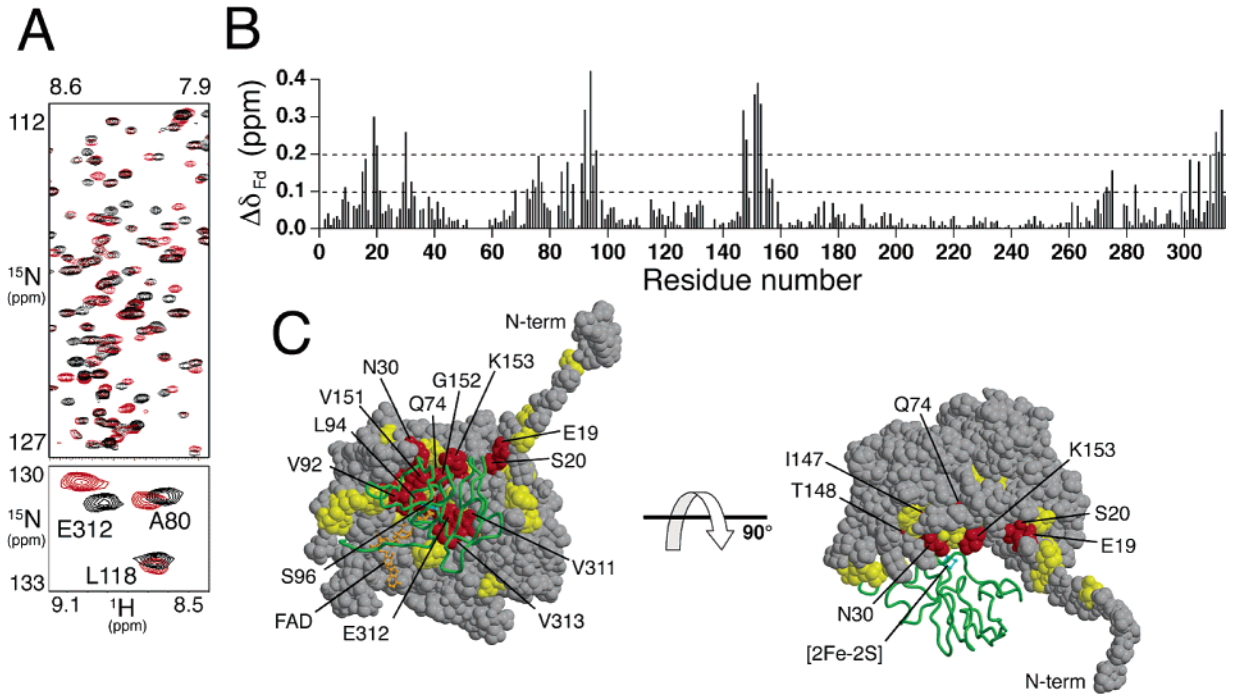

FIGURE 2: Chemical shift perturbation of FNR upon formation of the complex with Fd. (A) Superimposed $^1H-^{15}N$ HSQC spectra of free [^{15}N]FNR (black) and [^{15}N]FNR in a complex with unlabeled Fd (red) at pH 6.0. The top panel displays the same region as the inset in Figure 1A. The bottom panel shows a well-resolved part of the spectrum, displaying changes in the chemical shift values of the Ala80, Leu118, and Glu312 amide groups. (B) Plot of the weighted averages of the ^1H and ^{15}N chemical shift changes, calculated with the function $\Delta\delta_{Fd} = [(\Delta\delta_{^1H})^2 + 0.17(\Delta\delta_{^{15}N})^2]^{1/2}$. The absence of bars in the plot indicates unassigned residues, proline residues, or unmeasured shifts due to resonance overlaps. (C) Mapping of the perturbed residues on the crystal structure of the FNR−Fd complex (PDB entry 1GAQ). FNR is colored gray with the FAD cofactor displayed in an orange ball-and-stick model. The backbone of the bound Fd is displayed in green, and the [2Fe-2S] cluster in the Fd molecule is shown as a cyan ball-and-stick model. Red spheres indicate perturbed residues with $\Delta\delta_{Fd}$ values of >0.2 ppm, and yellow spheres show $\Delta\delta_{Fd}$ values of 0.1−0.2 ppm. The displayed N-terminal residues (I1−K18) of FNR were generated by a molecular dynamics simulation with Insight II (MSI) to map the perturbed residues onto the flexible N-terminal region, for which X-ray diffraction was not observed. The right figure is drawn by rotating the left one along the *X*-axis by 90°.

binding of Fd. We prepared two truncated forms of FNR lacking the first 23 residues (Δ23-FNR) and the first 13 residues (Δ13-FNR) of the maize leaf FNR by mutagenesis. Figure 3A displays the sequences of the N-terminal regions of various leaf FNRs. In the sequences, Ala3, Glu9, Ala10, Pro11, Ala12, Lys18, Ser20, Lys21, and Lys22 are well conserved among the N-terminal regions of the leaf species. Figure 3B shows SDS−PAGE patterns of the highly expressed various lengths of FNR overexpressed in *E. coli* cells. The differences observed in the electrophoretic mobility of the variants were consistent with the lengths of the polypeptides, as shown by the calculated molecular mass of each polypeptide, 32 788 Da for Δ23-FNR, 34 013 Da for Δ13-FNR, and 35 249 Da for wild-type FNR. Figure 3C shows the last step of purification. Although wild-type FNR was able to bind to the Fd-immobilized column even at a Tris-HCl concentration of 50 mM, Δ13- and Δ23-FNRs were unable to bind to the column under the same conditions. At 5 mM Tris-HCl, Δ13- and Δ23-FNRs had a moderate and slight affinity, respectively, for the column. Thus, while Δ13-FNR with a high purity was obtained, the purity of Δ23-FNR was not complete. A $^1H-^{15}N$ HSQC spectrum of the ^{15}N-labeled Δ13-FNR showed that the mutant retains its native conformation (Supporting Information). On the other hand, the quality of the HSQC spectrum of Δ23-FNR was not good enough (data not shown). It remains unknown if the low quality is caused by the low purity of Δ23-FNR or its partial unfolding. Nevertheless, both mutants expressed by the cultured *E. coli* bound FAD as the cofactor, suggesting that they retain the native conformation. Thus, it is likely that the observed decrease in affinity with the Fd-immobilized column represents the fact that some N-terminal residues of FNR are responsible for binding to Fd.

Comparison between NADP$^+$- and Inhibitor-Bound States of FNR. We analyzed the binding mechanism of FNR for NADP$^+$. In addition, we examined the binding site of adenosine 2′,5′-diphosphate, which lacks the nicotinamide mononucleotide of NADP$^+$ and acts as a competitive inhibitor with NADP$^+$ for FNR (*2*).

Figure 4A shows the chemical structures of the ligands and the perturbed levels of the FNR residues upon ligand binding. When NADP$^+$ and the inhibitor bind, 38 and 31 amide chemical shifts are significantly changed, respectively. In addition, 11 peaks disappeared in the exchange between NADP$^+$-bound and free states, and seven peaks in the exchange between the inhibitor-bound and free states (Figure 4A,B). The plot pattern of the perturbation levels shows that the residues of the peaks that disappeared are located among the residues whose resonance positions shifted greatly, indicating that the residues of the broadened peaks can be classified as being significantly perturbed (Figure 4A).

Differences in the spectra of the NADP$^+$- and inhibitor-bound states were observed in the C-terminal active site of FNR. As shown in the spectra, the peak of Thr172 disappeared completely in the inhibitor-bound state as well as in the NADP$^+$-bound state, but the peak of Tyr314 remained in the inhibitor-bound state (Figure 4B). Figure 4C shows the mapping of the residues with appreciable changes upon

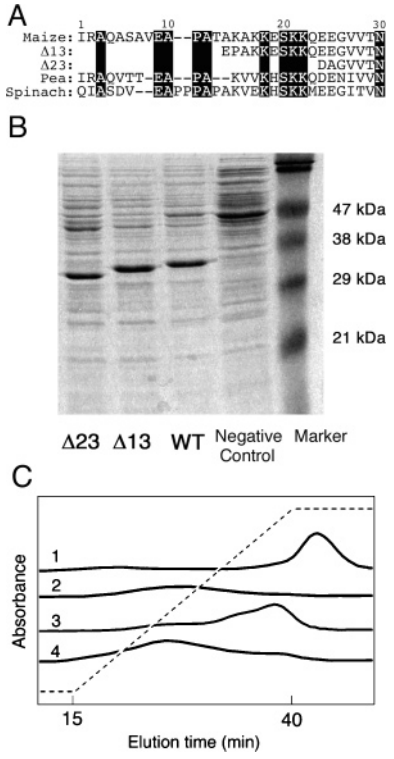

FIGURE 3: N-Terminal binding site of FNR. (A) Sequence alignment of the N-terminal regions of FNRs and the constructions of truncated recombinant Δ13 and Δ23 maize leaf FNRs. (B) SDS−PAGE gel patterns of the *E. coli* sedimentations that overexpressed the wild-type and truncated forms of FNRs, stained with Coomassie Brilliant Blue. A negative control was prepared by transforming bacteria with a vector carrying no FNR-related gene. (C) Elution profiles of wild-type, Δ13, and Δ23 FNRs from the Fd-immobilized Sepharose column: (1) wild-type with a 5 mM Tris-HCl buffer, (2) Δ13 with a 50 mM Tris-HCl buffer, (3) Δ13 with a 5 mM Tris-HCl buffer, and (4) Δ23 with a 5 mM Tris-HCl buffer. The solution containing each kind of FNR was loaded onto a Fd-immobilized resin (bed volume, 50 mL), which was equilibrated in advance at pH 7.5 and 4 °C, and the proteins were eluted by the application of a linear gradient of 0 to 500 mM NaCl at a flow rate of 2 mL/min. It should be noted that the period for the salt gradient was started as soon as the sample was loaded, without the usual washing procedure, and that the elution in the gradient period could, therefore, include passed-through proteins. This is because the affinity of FNR for the ferredoxin column was not so high that even the wild-type FNR must be eluted without the washing procedure.

each ligand binding on the X-ray crystal structure. Peaks that disappeared approximately correspond to the contact residues found at the binding sites for the ligands in previous structural studies (*18*, *37*, *38*). In addition, residues perturbed upon NADP$^+$ binding, but not upon inhibitor binding (Ser96, Gly173, Gly273, Glu312, and Tyr314), were mapped on the active center, which is composed of both the C-terminal region of FNR and the isoalloxazine ring of FAD (Figure 4D), indicating that the nicotinamide mononucleotide of NADP$^+$ is accessible to the center of the electron-transferring reaction.

NADP$^+$-Binding Region Analyzed by a Titration Experiment. We carried out a titration experiment to characterize NADP$^+$ binding. As the concentration of NADP$^+$ was increased, several perturbed peaks moved or disappeared in the ^{1}H−^{15}N HSQC spectra of [^{15}N]FNR (Figure 5A). From chemical shift changes of more than 0.2 ppm occurring in a fast exchange mode, we estimated the average dissociation constant for the NADP$^+$ binding to be 85 μM. We further analyzed the amide protons that exhibited broadened signals upon NADP$^+$ binding, and found that they were located closer to the ligand binding sites than the amide protons in the fast exchange mode (Figure 5B,C). These line broadening effects of the resonances were site-specific, as observed in Gln248 and Glu312. The drastically weakened signals correspond to the region of interaction with the adenosine portion, 2′-phosphate, and 5′-phosphate of NADP$^+$, whereas the less significantly weakened signals correspond to the region of interaction with the nicotinamide mononucleotide of the NADP$^+$. This result implies the accumulation of at least two species of FNR−NADP$^+$ complexes during titration (see Discussion).

DISCUSSION

We have assigned the backbone amide resonances of FNR. A combination of advanced NMR techniques and well-dispersed spectra allowed us to assign the backbone resonances of this 35 kDa monomeric protein. Our NMR analyses showed that the N-terminal residues had chemical shifts typical of disordered random coils and transverse relaxation rates much slower than those for the other rigid part. We have previously shown that the intact maize leaf FNR has a fluctuating tail protruding into the solvent in a small-angle X-ray scattering analysis (*39*). The mutant in which the N-terminal region was truncated and the enzyme in which the same region was proteolytically digested were fully active in the NADPH diaphorase assay, but lost the ability to interact with Fd (*40*, *41*).

NMR analyses and truncation studies suggested that the interaction motif with Fd lies around Glu10 and/or Ser20. Both motifs of EA- -PA around Glu10 and KxSKK in the N-terminal region appear to be crucial for higher-plant leaf FNRs. The N-terminal region of FNR might interact with an acidic α-helix running from Tyr23 to Asp29 in Fd (*42*). In the previous NMR study using [^{15}N]Fd, Ile24 and Gln27 of Fd were largely perturbed upon binding of nonlabeled FNR (*16*). This interaction would be of a moderate strength, because the complex formation involving the N-terminal tail of FNR was not observed in the crystal structure and the cross-link found between the α-NH_2 of the N-terminal residue of FNR and Fd was minor (*42*). The K_m value of FNR for Fd is 3.3 μM at 25 °C (*9*), which contributes to the fast exchange mode at 40 °C (*36*). The cyanobacterium *Anabaena* FNR has the TQAKAK motif instead of the N-terminal sequence found in the plant type, and the basic charges in the lysine side chains are needed for formation of the intermediate complex with Fd at low ionic strengths (*43*). The absence of such N-terminal basic motifs may explain the low catalytic efficiency of *E. coli* FNR (*5*). Other than the N-terminal region, *Anabaena* FNR contains 11 residues that are important for the interaction with Fd, including five lysine and two arginine residues involved in catalytic function (*44*). The basic residues in the N-terminal region of FNR may play a role in recognizing acidic Fd so that the initial intermediate complex is formed between FNR and Fd. According to our results, the chemical shifts of Glu19 and Ser20 were largely perturbed upon complex formation with Fd, although they do not exist on the interaction surface determined from the crystal structure. Nearby residues, Lys22 and Gln23, exhibited small perturbations suggesting that the

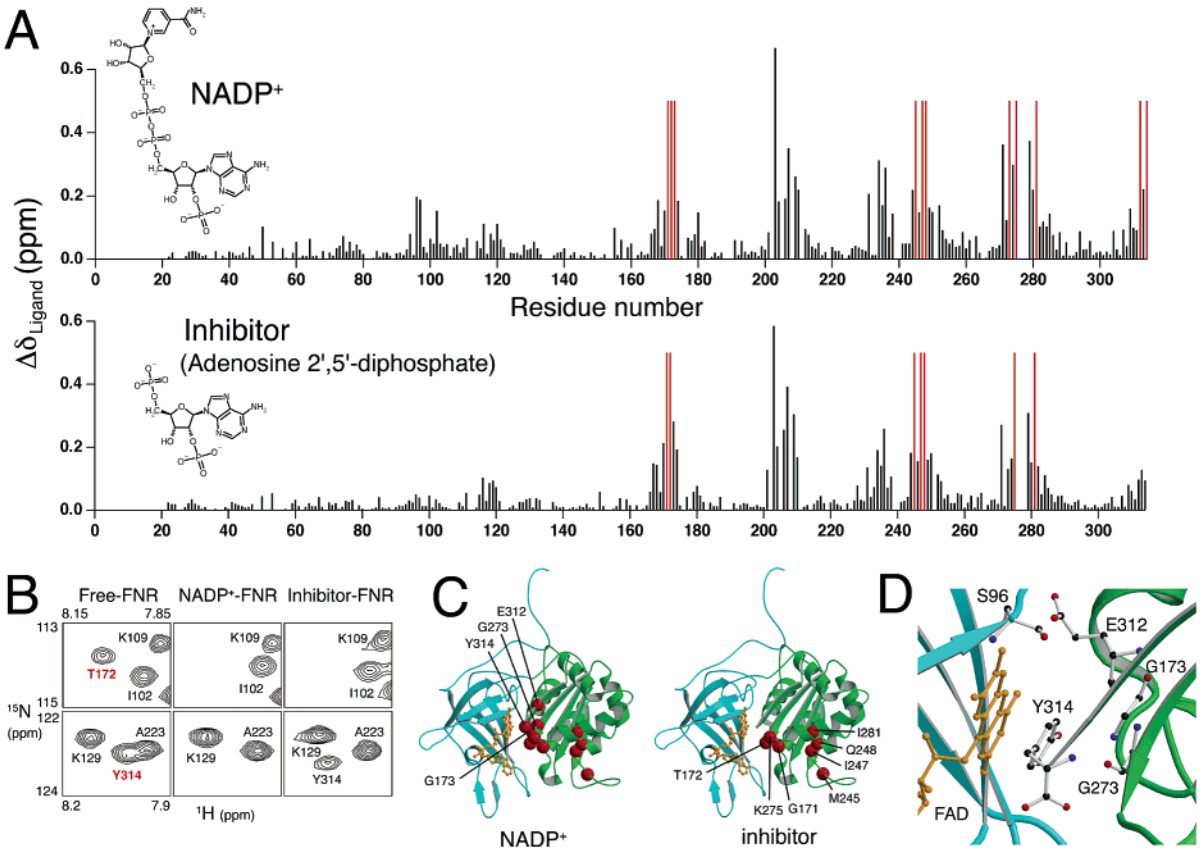

FIGURE 4: Comparison between the binding effects of NADP$^+$ and an analogue inhibitor. (A) Plots of the ^{1}H and ^{15}N chemical shift changes of FNR at pH 8.0 upon binding to NADP$^+$ (top) and to an analogue inhibitor, adenosine 2′,5′-diphosphate (bottom), calculated as a function of $\Delta\delta_{ligand} = [(\Delta\delta^1_H)^2 + 0.17(\Delta\delta^{15}_N)^2]^{1/2}$. The chemical structures of NADP$^+$ and the inhibitor are drawn on the left. Since the addition of NADP$^+$ did not significantly perturb the chemical shifts of FNR around pH 6, the experiment was carried out at pH 8.0. The relatively high pH value consequently made the amide signals from the flexible N-terminal region unobservable. Red bars indicate broadened resonances beyond detection because of an intermediate rate exchange between ligand binding and dissociation. (B) Comparison of parts of ^{1}H−^{15}N HSQC spectra in the free and ligand-bound states of FNR at pH 8.0. The disappearance of the peaks was most likely caused by the dynamic processes on microsecond to millisecond time scales. (C) Mapping of the residues for which the resonances were broadened upon binding to the ligands on the X-ray structure (PDB entry 1GAW). The FAD-binding domain is colored cyan and the NADP$^+$-binding domain green. The bound FAD cofactor is displayed as an orange ball-and-stick model. Red spheres show amide protons that disappeared, indicating that they are closest to the NADP$^+$ (left) or inhibitor (right) binding sites. (D) Close-up view of the C-terminal electron transfer center of FNR oriented as in panel C. The residues that exhibited large chemical shift perturbations upon NADP$^+$ binding but small ones upon inhibitor binding (Ser96, Gly173, Gly273, Glu312, and Tyr314) are shown as a ball-and-stick model.

joint region of the N-terminal tail does not change their conformations drastically. Therefore, the large perturbation observed in Glu19 and Ser20 may be caused by another reason; for example, Fd might contact Glu19 through electric interaction to make an initial nonproductive complex. In another species with the reported X-ray crystallographic structure, *Anabaena* Fd also binds to the N-terminal FAD binding domain and to the C-terminus of *Anabaena* FNR (*15*). The intermolecular hydrogen-bonding residues of the *Anabaena* FNR−Fd complex, Asn13, Lys75, Val136, Arg264, Glu267, Lys293, Val300, Glu301, and Thr302 in *Anabaena* FNR, correspond to Asn30, Lys91, Val151, Lys275, Glu278, K304, Val311, Glu312, and Val313, respectively, in maize leaf FNR, which is consistent with NMR analysis. Despite being located on the inside of the FNR molecule, Gln74, Ile147, and Thr148 exhibited chemical shift perturbations as large as those for residues on the ferredoxin-binding surface (Figure 2B). Interestingly, the perturbation pattern upon Fd binding may indicate an alteration of the atomic environment on the periphery of FAD. The residue for which the chemical shift is most largely perturbed was Leu94, and it is adjacent to Tyr95 whose aromatic ring lies against the *si* face of the isoalloxazine ring of FAD. Therefore, when Fd binds, a slight conformational change may occur around FAD, and the propagation of the conformational change from the active site to β4 (Arg93−Ser96), β3 (Ser75−Ile79), and β6 (Asn144−Val151) strands in the FAD binding domain may perturb the chemical shifts of Gln74, Ile147, and Thr148.

We identified the binding region of FNR and NADP$^+$. The position that the aromatic side chain of Tyr314 takes in the free form of FNR corresponds to the position that the nicotinamide group of NADP$^+$ takes in the complex form, being close and parallel to the *re* face of FAD (Figure 4D) (*11*). For the electron transfer step following NADP$^+$ binding, the nicotinamide group is expected to occupy the place of the aromatic side chain of Tyr314 in the free form (*4*, *14*). Therefore, the nicotinamide group should interact with the bulky tyrosine residue, and thermal fluctuation may cause some structural rearrangements by flipping out the side chain of Tyr314 or the C-terminal backbone in solution. Many FNR-like flavoproteins take advantage of the flavin-shielding system (*45*−*50*). In the titration experiments with NADP$^+$, the nicotinamide mononucleotide (NMN) binding region

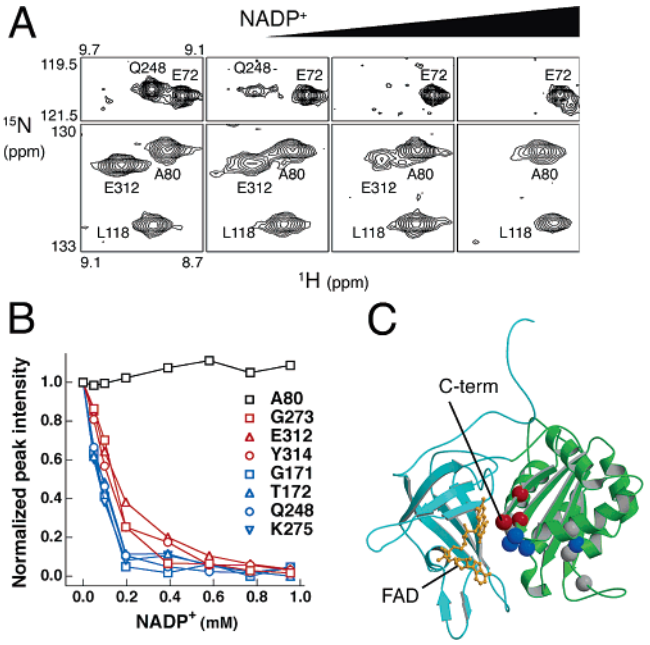

FIGURE 5: Broadening effect of FNR in NADP$^+$ titration. (A) Examples of ^{1}H−^{15}N HSQC spectra of 0.9 mM [^{15}N]FNR during titration with NADP$^+$ at pH 8.0. From left to right, NADP$^+$ was added so that its concentration reached 0, 0.2, 0.39, and 0.95 mM, respectively. Gln248 and Glu312 are in intermediate rate exchange on the NMR time scale, which made the peaks unobservable at higher concentrations of NADP$^+$. (B) Changes in peak intensity of the broadened signals by titration with NADP$^+$. Blue symbols and lines for Gly171, Thr172, Gln248, and Lys275 indicate the drastically weakened signals during the titration, while red symbols and lines for Gly273, Glu312, and Tyr314 are the gradually weakened signals. The signal intensities were normalized so that the intensities of three peaks derived from residues Leu31, Glu72, and Ala80, which resonated apart from each other in the spectrum and were clearly irrelevant to the interaction with NADP$^+$, became uniform. (C) Mapping of the amide protons that had different broadening effects upon NADP$^+$ binding. Broadened amide groups are mapped onto the structure of FNR, colored as in panel B. Peaks that were difficult to analyze because of overlapping (Gly173, Met245, and Ile281) and an intrinsically weak resonance (Ile247) are shown as gray spheres.

exhibited more moderate broadening effects than the 2′,5′-diphosphate binding region. This phenomenon suggests a bipartite mechanism of the binding of NADP$^+$ to FNR as shown in eq 1:

$$\text{FNR} + \text{NADP}^+ \rightarrow \text{FNR}-[2',5'\text{-diphosphates}]\text{-}[\text{NMN}] \rightarrow \text{FNR}-\text{NADP}^+ \quad (1)$$

where FNR−[2′,5′-diphosphates]-[NMN] represents the intermediate in which the 2′,5′-diphosphates of NADP$^+$ are adjacent to the polypeptide; however, the nicotinamide moiety does not yet reach the C-terminal region, and as more NADP$^+$ is added, more of the final complex accumulates. A similar bipartite mechanism has been also proposed by Carrillo and Ceccarelli (*4*). Although we have proposed a two-step binding mechanism from the two kinds of line broadening effects, an alternative interpretation is also possible where the binding affinity is uniform and the region-dependent line broadening effects are observed only because of the different chemical shift changes ($\Delta\delta$) in the interaction sites upon binding of NADP$^+$. Since the apparent transverse relaxation rate, namely, the line broadening effect, is generally a function of both the associated exchange rate, k_{ex}, and chemical shift change, $\Delta\delta$, determination of whether the two-step binding is correct requires further detailed analyses taking $\Delta\delta$ into consideration. We did not find any new peaks appearing when NADP$^+$ was added at a concentration as high as 12.4 mM to 0.9 mM [^{15}N]FNR. Therefore, even at a high concentration of NADP$^+$, the binding of NADP$^+$ to FNR was still in an intermediate rate exchange mode. This may be because of the relatively high temperature of 40 °C. Although some new peaks were expected to be observed at lower temperatures, the peak broadening in the spectra prevented analysis. Alternatively, there may be an additional intermediate rate exchange in the binding between FNR and NADP$^+$.

In conclusion, we have assigned almost all the NMR backbone resonances of a 314-residue maize leaf FNR. The chemical shift perturbation upon formation of the complex with a maize ferredoxin indicated that a flexible N-terminal region of FNR was involved in the interaction with ferredoxin, and the interaction was further confirmed by analysis using N-terminally truncated mutants of FNR. By comparing the spectra of FNR in the NADP$^+$- and inhibitor-bound states, we found that the nicotinamide moiety of NADP$^+$ is accessible to the C-terminal Tyr314. We propose that the interactions of the N- and C-terminal segments with ferredoxin and NADP$^+$, respectively, lead to the formation of the catalytic competent complex of FNR and its substrates. Since the ends of the polypeptide chain act as flexible regions of proteins, they may contribute to the search for a larger space for a binding partner (*51*) and to the opening of the active sites.

ACKNOWLEDGMENT

We thank Drs. H. Akutsu and H. Yagi (Institute for Protein Research) for assistance in the NMR facility and K. Teshima (Hiroshima University, Hiroshima, Japan) and T. Endo (Nagoya University, Nagoya, Japan) for helpful discussions.

SUPPORTING INFORMATION AVAILABLE

Superimposed ^{1}H−^{15}N HSQC spectra of WT-FNR (blue) and Δ13-FNR (Figure S1) and chemical shifts for FNR at pH 6.5 (Table S1). This material is available free of charge via the Internet at http://pubs.acs.org.

REFERENCES

1. Shin, M., and Arnon, D. I. (1965) Enzymic mechanisms of pyridine nucleotide reduction in chloroplasts, *J. Biol. Chem. 240*, 1405−1411.
2. Batie, C. J., and Kamin, H. (1984) Ferredoxin:NADP$^+$ oxidoreductase. Equilibria in binary and ternary complexes with NADP$^+$ and ferredoxin, *J. Biol. Chem. 259*, 8832−8839.
3. Arakaki, A. K., Ceccarelli, E. A., and Carrillo, N. (1997) Plant-type ferredoxin-NADP$^+$ reductases: A basal structural framework and a multiplicity of functions, *FASEB J. 11*, 133−140.
4. Carrillo, N., and Ceccarelli, E. A. (2003) Open questions in ferredoxin-NADP$^+$ reductase catalytic mechanism, *Eur. J. Biochem. 270*, 1900−1915.
5. Ceccarelli, E. A., Arakaki, A. K., Cortez, N., and Carrillo, N. (2004) Functional plasticity and catalytic efficiency in plant and bacterial ferredoxin-NADP(H) reductases, *Biochim. Biophys. Acta 1698*, 155−165.
6. Hanukoglu, I., and Gutfinger, T. (1989) cDNA sequence of adrenodoxin reductase. Identification of NADP$^+$-binding sites in oxidoreductases, *Eur. J. Biochem. 180*, 479−484.
7. Chen, Y. P., and Yoch, D. C. (1989) Isolation, characterization and biological activity of ferredoxin-NAD$^+$ reductase from the

methane oxidizer *Methylosinus trichosporium* OB3b, *J. Bacteriol. 171*, 5012−5016.
8. Bianchi, V., Reichard, P., Eliasson, R., Pontis, E., Krook, M., Jörnvall, H., and Haggård-Ljungquist, E. (1993) *Escherichia coli* ferredoxin-NADP$^+$ reductase: Activation of *E. coli* anaerobic ribonucleotide reduction, cloning of the gene (fpr), and overexpression of the protein, *J. Bacteriol. 175*, 1590−1595.
9. Onda, Y., Matsumura, T., Kimata-Ariga, Y., Sakakibara, H., Sugiyama, T., and Hase, T. (2000) Differential interaction of maize root ferredoxin:NADP$^+$ oxidoreductase with photosynthetic and non-photosynthetic ferredoxin isoproteins, *Plant Physiol. 123*, 1037−1045.
10. Aliverti, A., Faber, R., Finnerty, C. M., Ferioli, C., Pandini, V., Negri, A., Karplus, P. A., and Zanetti, G. (2001) Biochemical and crystallographic characterization of ferredoxin-NADP$^+$ reductase from nonphotosynthetic tissues, *Biochemistry 40*, 14501−14508.
11. Karplus, P. A., Daniels, M. J., and Herriott, J. R. (1991) Atomic structure of ferredoxin-NADP$^+$ reductase: Prototype for a structurally novel flavoenzyme family, *Science 251*, 60−66.
12. Serre, L., Vellieux, F. M., Medina, M., Gomez-Moreno, C., Fontecilla-Camps, J. C., and Frey, M. (1996) X-ray structure of the ferredoxin:NADP$^+$ reductase from the cyanobacterium *Anabaena* PCC 7119 at 1.8 Å resolution, and crystallographic studies of NADP$^+$ binding at 2.25 Å resolution, *J. Mol. Biol. 263*, 20−39.
13. Ingelman, M., Bianchi, V., and Eklund, H. (1997) The three-dimensional structure of flavodoxin reductase from *Escherichia coli* at 1.7 Å resolution, *J. Mol. Biol. 268*, 147−157.
14. Deng, Z., Aliverti, A., Zanetti, G., Arakaki, A. K., Ottado, J., Orellano, E. G., Calcaterra, N. B., Ceccarelli, E. A., Carrillo, N., and Karplus, P. A. (1999) A productive NADP$^+$ binding mode of ferredoxin-NADP$^+$ reductase revealed by protein engineering and crystallographic studies, *Nat. Struct. Biol. 6*, 847−853.
15. Morales, R., Charon, M. H., Kachalova, G., Serre, L., Medina, M., Gómez-Moreno, C., and Frey, M. (2000) A redox-dependent interaction between two electron-transfer partners involved in photosynthesis, *EMBO Rep. 1*, 271−276.
16. Kurisu, G., Kusunoki, M., Katoh, E., Yamazaki, T., Teshima, K., Onda, Y., Kimata-Ariga, Y., and Hase, T. (2001) Structure of the electron-transfer complex between ferredoxin and ferredoxin-NADP$^+$ reductase, *Nat. Struct. Biol. 8*, 117−121.
17. Hurley, J. K., Faro, M., Brodie, T. B., Hazzard, J. T., Medina, M., Gómez-Moreno, C., and Tollin, G. (2000) Highly nonproductive complexes with *Anabaena* ferredoxin at low ionic strength are induced by nonconservative amino acid substitutions at Glu139 in *Anabaena* ferredoxin:NADP$^+$ reductase, *Biochemistry 39*, 13695−13702.
18. Hermoso, J. A., Mayoral, T., Faro, M., Gómez-Moreno, C., Sanz-Aparicio, J., and Medina, M. (2002) Mechanism of coenzyme recognition and binding revealed by crystal structure analysis of ferredoxin-NADP$^+$ reductase complexed with NADP$^+$, *J. Mol. Biol. 319*, 1133−1142.
19. Orellano, E. G., Calcaterra, N. B., Carrillo, N., and Ceccarelli, E. A. (1993) Probing the role of the carboxyl-terminal region of ferredoxin-NADP$^+$ reductase by site-directed mutagenesis and deletion analysis, *J. Biol. Chem. 268*, 19267−19273.
20. Yamazaki, T., Lee, W., Arrowsmith, C. H., Muhandiram, D. R., and Kay, L. E. (1994) A suite of triple resonance NMR experiments for the backbone assignment of ^{15}N, ^{13}C, ^{2}H labeled proteins with high sensitivity, *J. Am. Chem. Soc. 116*, 11655−11666.
21. Pervushin, K., Riek, R., Wider, G., and Wüthrich, K. (1997) Attenuated T_2 relaxation by mutual cancellation of dipole−dipole coupling and chemical shift anisotropy indicates an avenue to NMR structures of very large biological macromolecules in solution, *Proc. Natl. Acad. Sci. U.S.A. 94*, 12366−12371.
22. Farmer, B. T., II, Constantine, K. L., Goldfarb, V., Friedrichs, M. S., Wittekind, M., Yanchunas, J., Jr., Robertson, J. G., and Mueller, L. (1996) Localizing the NADP$^+$ binding site on the MurB enzyme by NMR, *Nat. Struct. Biol. 3*, 995−997.
23. Tugarinov, V., Muhandiram, R., Ayed, A., and Kay, L. E. (2002) Four-dimensional NMR spectroscopy of a 723-residue protein: Chemical shift assignments and secondary structure of malate synthase G, *J. Am. Chem. Soc. 124*, 10025−10035.
24. Löhr, F., Katsemi, V., Hartleib, J., Günther, U., and Rüterjans, H. (2003) A strategy to obtain backbone resonance assignments of deuterated proteins in the presence of incomplete amide ^{2}H/^{1}H back-exchange, *J. Biomol. NMR 25*, 291−311.
25. Salzmann, M., Pervushin, K., Wider, G., Senn, H., and Wüthrich, K. (1998) TROSY in triple-resonance experiments: New perspectives for sequential NMR assignment of large proteins, *Proc. Natl. Acad. Sci. U.S.A. 95*, 13585−13590.
26. Salzmann, M., Wider, G., Pervushin, K., Senn, H., and Wüthrich, K. (1999) TROSY-type triple-resonance experiments for sequential NMR assignments of large proteins, *J. Am. Chem. Soc. 121*, 844−848.
27. Cavanagh, J., Fairbrother, W. J., Palmar, A. G., III, and Skelton, N. J. (1996) *Protein NMR Spectroscopy*: *Principles and Practice*, Academic Press, San Diego.
28. Delaglio, F., Grzesiek, S., Vuister, G. W., Zhu, G., Pfeifer, J., and Bax, A. (1995) NMRpipe: A multidimensional spectral processing system based on UNIX pipes, *J. Biomol. NMR 6*, 277−293.
29. Garrett, D. S., Powers, R., Gronenborn, A. M., and Clore, G. M. (1991) A common sense approach to peak picking in two, three and four-dimensional spectra using automatic computer analysis of contour diagrams, *J. Magn. Reson. 95*, 214−220.
30. Wishart, D. S., and Sykes, B. D. (1994) Chemical shifts as a tool for structure determination, *Methods Enzymol. 239*, 363−392.
31. Hase, T., Mizutani, S., and Mukohata, Y. (1991) Expression of maize ferredoxin cDNA in *Escherichia coli*, *Plant Physiol. 97*, 1395−1401.
32. Kraulis, P. J. (1991) MOLSCRIPT: A program to produce both detailed and schematic plots of protein structures, *J. Appl. Crystallogr. 24*, 946−950.
33. Merritt, E. A., and Bacon, D. J. (1997) Raster3D: Photorealistic molecular graphics, *Methods Enzymol. 277*, 505−524.
34. Hall, D. A., VanderKooi, C. W., Stasik, C. N., Stevens, S. Y., Zuiderweg, E. R., and Matthews, R. G. (2001) Mapping the interactions between flavodoxin and its physiological partners flavodoxin reductase and cobalamin-dependent methionine synthase, *Proc. Natl. Acad. Sci. U.S.A. 98*, 9521−9526.
35. Aliverti, A., Deng, Z., Ravasi, D., Piubelli, L., Karplus, P. A., and Zanetti, G. (1998) Probing the function of the invariant glutamyl residue 312 in spinach ferredoxin-NADP$^+$ reductase, *J. Biol. Chem. 273*, 34008−34015.
36. Zuiderweg, E. R. (2002) Mapping protein−protein interactions in solution by NMR spectroscopy, *Biochemistry 41*, 1−7.
37. Karplus, P. A., and Bruns, C. M. (1994) Structure−function relations for ferredoxin reductase, *J. Bioenerg. Biomembr. 26*, 89−99.
38. Bruns, C. M., and Karplus, P. A. (1995) Refined crystal structure of spinach ferredoxin reductase at 1.7 Å resolution: Oxidized, reduced and 2′-phospho-5′-AMP bound states, *J. Mol. Biol. 247*, 125−145.
39. Maeda, M., Hamada, D., Hoshino, M., Onda, Y., Hase, T., and Goto, Y. (2002) Partially folded structure of flavin adenine dinucleotide-depleted ferredoxin-NADP$^+$ reductase with residual NADP$^+$ binding domain, *J. Biol. Chem. 277*, 17101−17107.
40. Aliverti, A., Jansen, T., Zanetti, G., Ronchi, S., Herrmann, R. G., and Curti, B. (1990) Expression in *Escherichia coli* of ferredoxin: NADP$^+$ reductase from spinach. Bacterial synthesis of the holoflavoprotein and of an active enzyme form lacking the first 28 amino acid residues of the sequence, *Eur. J. Biochem. 191*, 551−555.
41. Gadda, G., Aliverti, A., Ronchi, S., and Zanetti, G. (1990) Structure−function relationship in spinach ferredoxin-NADP$^+$ reductase as studied by limited proteolysis, *J. Biol. Chem. 265*, 11955−11959.
42. Zanetti, G., Morelli, D., Ronchi, S., Negri, A., Aliverti, A., and Curti, B. (1988) Structural studies on the interaction between ferredoxin and ferredoxin-NADP$^+$ reductase, *Biochemistry 27*, 3753−3759.
43. Hurley, J. K., Fillat, M. F., Gómez-Moreno, C., and Tollin, G. (1996) Electrostatic and hydrophobic interactions during complex formation and electron transfer in the ferredoxin/ferredoxin: NADP$^+$ reductase system from *Anabaena*, *J. Am. Chem. Soc. 118*, 5526−5531.
44. Hurley, J. K., Morales, R., Martínez-Júlvez, M., Brodie, T. B., Medina, M., Gómez-Moreno, C., and Tollin, G. (2002) Structure−function relationships in *Anabaena* ferredoxin/ferredoxin:NADP$^+$ reductase electron transfer: Insights from site-directed mutagenesis, transient absorption spectroscopy and X-ray crystallography, *Biochim. Biophys. Acta 1554*, 5−21.

45. Pai, E. F., Karplus, P. A., and Schulz, G. E. (1988) Crystallographic analysis of the binding of NADPH, NADPH fragments, and NADPH analogues to glutathione reductase, *Biochemistry 27*, 4465−4474.
46. Calcaterra, N. B., Picó, G. A., Orellano, E. G., Ottado, J., Carrillo, N., and Ceccarelli, E. A. (1995) Contribution of the FAD binding site residue tyrosine 308 to the stability of pea ferredoxin-NADP$^+$ oxidoreductase, *Biochemistry 34*, 12842−12848.
47. Hubbard, P. A., Shen, A. L., Paschke, R., Kasper, C. B., and Kim, J. J. (2001) NADPH-cytochrome P450 oxidoreductase. Structural basis for hydride and electron transfer, *J. Biol. Chem. 276*, 29163−29170.
48. Adak, S., Sharma, M., Meade, A. L., and Stuehr, D. J. (2002) A conserved flavin-shielding residue regulates NO synthase electron transfer and nicotinamide coenzyme specificity, *Proc. Natl. Acad. Sci. U.S.A. 99*, 13516−13521.
49. Chatwood, L. L., Müller, J., Gross, J. D., Wagner, G., and Lippard, S. J. (2004) NMR structure of the flavin domain from soluble methane monooxygenase reductase from *Methylococcus capsulatus* (Bath), *Biochemistry 43*, 11983−11991.
50. Nogués, I., Tejero, J., Hurley, J. K., Paladini, D., Frago, S., Tollin, G., Mayhew, S. G., Gómez-Moreno, C., Ceccarelli, E. A., Carrillo, N., and Medina, M. (2004) Role of the C-terminal tyrosine of ferredoxin-nicotinamide adenine dinucleotide phosphate reductase in the electron transfer processes with its protein partners ferredoxin and flavodoxin, *Biochemistry 43*, 6127−6137.
51. Shoemaker, B. A., Portman, J. J., and Wolynes, P. G. (2000) Speeding molecular recognition by using the folding funnel: The fly-casting mechanism, *Proc. Natl. Acad. Sci. U.S.A. 97*, 8868−8873.

BI050424B